

Longitudinal brain atlases of early developing cynomolgus macaques from birth to 48 months of age

Tao Zhong^{a,d,1}, Jingkuan Wei^{b,f,1}, Kunhua Wu^c, Liangjun Chen^a, Fenqiang Zhao^a, Yuchen Pei^a, Ya Wang^a, Hongjiang Zhang^c, Zhengwang Wu^a, Ying Huang^a, Tengfei Li^a, Li Wang^a, Yongchang Chen^{b,f}, Weizhi Ji^{b,f}, Yu Zhang^d, Gang Li^{a,*}, Yuyu Niu^{b,e,f,**}

^a Department of Radiology and BRIC, University of North Carolina Chapel Hill, USA

^b State Key Laboratory of Primate Biomedical Research, Institute of Primate Translational Medicine, Kunming University of Science and Technology, Kunming, China

^c Department of MRI, the First People's Hospital of Yunnan Province, Kunming, China

^d Guangdong Provincial Key Laboratory of Medical Image Processing, School of Biomedical Engineering, Southern Medical University, Guangzhou, China

^e Faculty of Life Science and Technology, Kunming University of Science and Technology, Kunming, China

^f Yunnan Key Laboratory of Primate Biomedical Research, Kunming, China

ARTICLE INFO

Keywords:

Longitudinal brain atlases

MRI

Cynomolgus macaque

Early brain development

ABSTRACT

Longitudinal brain imaging atlases with densely sampled time-points and ancillary anatomical information are of fundamental importance in studying early developmental characteristics of human and non-human primate brains during infancy, which feature extremely dynamic imaging appearance, brain shape and size. However, for non-human primates, which are highly valuable animal models for understanding human brains, the existing brain atlases are mainly developed based on adults or adolescents, denoting a notable lack of temporally densely-sampled atlases covering the dynamic early brain development. To fill this critical gap, in this paper, we construct a comprehensive set of longitudinal brain atlases and associated tissue probability maps (gray matter, white matter, and cerebrospinal fluid) with totally 12 time-points from birth to 4 years of age (i.e., 1, 2, 3, 4, 5, 6, 9, 12, 18, 24, 36, and 48 months of age) based on 175 longitudinal structural MRI scans from 39 typically-developing cynomolgus macaques, by leveraging state-of-the-art computational techniques tailored for early developing brains. Furthermore, to facilitate region-based analysis using our atlases, we also provide two popular hierarchy parcellations, i.e., cortical hierarchy maps (6 levels) and subcortical hierarchy maps (6 levels), on our longitudinal macaque brain atlases. These early developing atlases, which have the densest time-points during infancy (to the best of our knowledge), will greatly facilitate the studies of macaque brain development.

1. Introduction

Non-human primate models are widely employed to conduct comparative analysis in various human psychiatry and neuropathology studies (Belmonte et al., 2015; Capitanio and Emborg, 2008; Malkova et al., 2006; Poo et al., 2016; Rilling, 2014). Among non-human primate models, cynomolgus macaque (*Macaca fascicularis*) is a well-studied model system with tangible translational advantages, due to its biological similarities with human beings, such as prolonged uterine development, single pregnancy offspring, and the mature stage of the brain at birth. In both humans and cynomolgus macaques, early postnatal brain development is a complex, dynamic, and regionally heterogeneous process,

which is especially important for later brain structural, functional and cognitive results (Knickmeyer et al., 2008; Li et al., 2014a,b, 2019; Nie et al., 2013; Scott et al., 2016; Uematsu et al., 2012; Wang et al., 2019). To better study the mechanisms of brain development and evolution, a primary method is to compare the characteristics of early brain neurodevelopment between humans and macaques (Seidlitz et al., 2018; Wang et al.; Xia et al., 2020). Besides, the emerging gene-edited models of neurodevelopmental disorders in macaque monkeys have remarkably promoted the understanding of brain developmental mechanisms and the development of potential therapies for these disorders, especially in the precursor stage during early brain development (Chen et al., 2017; Jennings et al., 2016; Liu et al., 2016).

* Corresponding authors at: Department of Radiology and BRIC, University of North Carolina Chapel Hill, USA.

** Corresponding author at: State Key Laboratory of Primate Biomedical Research, Institute of Primate Translational Medicine, Kunming University of Science and Technology, Kunming, China.

E-mail addresses: gang.li@med.unc.edu (G. Li), niuyy@lpbr.cn (Y. Niu).

¹ Both the authors contributed equally to this work.

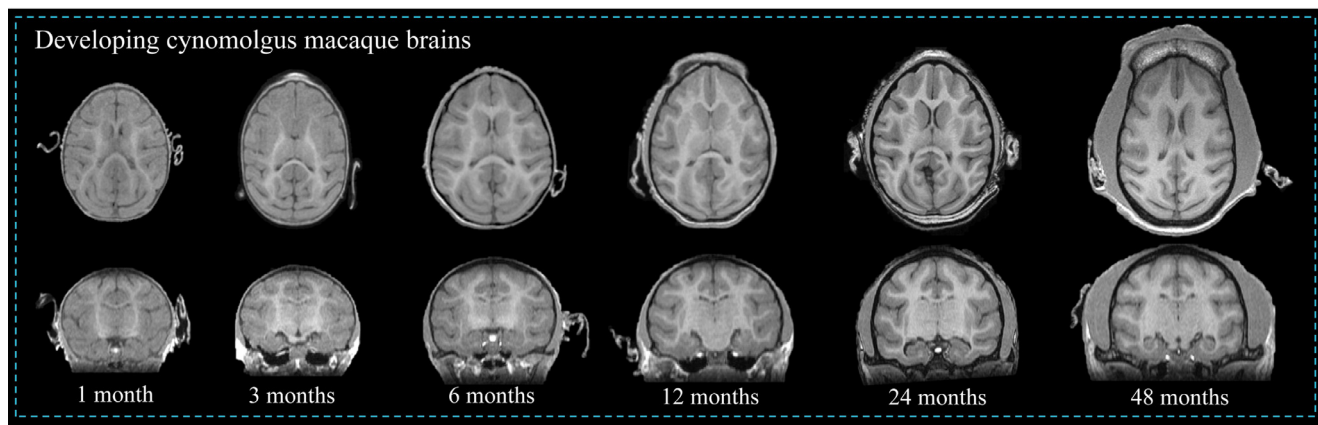


Fig. 1. Axial and coronal views of T1-weighted MR images of cynomolgus macaques at different ages.

Group analysis is a common method in MRI-based human brain studies, aiming to support scientific validity by improving statistical power and highlighting reliable neurological phenomena in a population (Friston et al., 1999). To achieve this, a common practice is to transform each subject's data into a common coordinate space, where a standard image of brain anatomy serves as a reference atlas or template (Mazziotta et al., 2001). These human brain atlases can be constructed based on the brain of an individual subject, such as the Colin N27 brain (Holmes et al., 1998); or the average of multiple individuals' anatomical structures, such as the ICBM152 atlas of Montreal Institute of Neurology (Mazziotta et al., 2001). However, a single brain atlas cannot capture the anatomical variation within the population. Therefore, population-average atlases are preferred for brain analysis at the population level, because they unbiasedly reflect the overall typical anatomical structures of the population with inter-individual variability. These atlases can then be used as the references to register new images to a common coordinate space, enabling the image normalization, comparison and analysis. Furthermore, regions of interest, such as tissue segmentation or brain parcellation (Rohlfing et al., 2012; Shi et al., 2014; Sun et al., 2021; Uus et al., 2021), can be outlined in template images and propagated to individual space for regional analysis.

Available MRI-based macaque brain atlases are mainly built from the adult or adolescent macaque population (Jung et al., 2020; Lv et al., 2020; McLaren et al., 2009; Quallo et al., 2010; Rohlfing et al., 2012; Weiss et al., 2020), as shown in Table 1. Therefore, they lack the sufficient capability to well capture the early postnatal brain development, which features extremely dynamic imaging contrast, brain appearance, shape, and size, as shown in Fig. 1. Two publicly available infant rhesus macaque atlases have been proposed to address these issues. One is the UNC-Emory Infant Atlases, which were constructed every three months during the first postnatal year for rhesus macaques (Shi et al., 2017). The other one is the ONPRC Infant Macaque Brain Atlases (Liu et al., 2019), which were constructed based on a cohort of 6 rhesus macaques scanned longitudinally at 2, 4, and 6 months of ages. However, both of them cannot precisely characterize the highly dynamic changes due to their sparse scan ages during the first year. Most importantly, they cannot well represent the infant cynomolgus macaques, due to remarkable inter-species brain differences in sulcal patterns, brain volume, and skull shape. For example, researchers have observed variation in the general morphology of the prelunate gyrus and sulcus (Van der Gucht et al., 2006) and surface differences in the frontal pole, ventral posterior frontal cortex and the temporal cortex (Frey et al., 2011) between two species. Besides, variations in the global brain volume within the *Macaca* genus (*fascicularis* < *mulatta* < *nemestrina*) (Malkova et al., 2006; McLaren et al., 2009) and skull shape (Frey et al., 2011) also suggested the need to have dedicated atlases for different species.

Therefore, there is a notable lack of publicly available 4D cynomolgus macaque brain atlases with densely sampled time-points covering the ages ranging from birth to adolescence (Song et al., 2021), due to the following two challenges. First, collecting individual MR images within the same homogeneous infant cohort at several densely sampled time-points remains a vital challenge, especially when the study is expected to cover a broad age range. Second, the extremely dynamic imaging contrast, brain appearance, shape, and size during early brain development of macaques pose a significant challenge in MR image processing. This study was designed to fill this critical gap by constructing the first set of brain volumetric atlases and their associated tissue probability maps (gray matter, white matter, and cerebrospinal fluid) at postnatal ages covering infant and part of adolescent periods, including a total of 12 age levels (i.e., 1, 2, 3, 4, 5, 6, 9, 12, 18, 24, 36, and 48 months). To achieve this, we apply our in-house developed techniques for infant brain tissue segmentation and developing macaque skull stripping (Li et al., 2014; Wang et al., 2015; Zhong et al., 2021), and a popular atlas-creation process (Avants et al., 2011; 2010), to a high-quality MRI dataset obtained by longitudinally scanning 39 typically developing cynomolgus macaques (*Macaca fascicularis*) at the age of 0 to 48 months. Meanwhile, we also created regional label maps based on the 6-level hierarchy parcellation maps from NMT v2 macaque brain template, including Cortical Hierarchy Atlas of the Rhesus Macaque (CHARM) and Subcortical Hierarchy Atlas of the Rhesus Macaque (SHARM) (Hartig et al., 2020; Jung et al., 2020). These 4D brain atlases will be reliable references and templates for neuroimaging studies of the early developing cynomolgus brains.

2. Materials and methods

2.1. Animal preparation

AAALAC International accredits the cynomolgus macaque (*Macaca fascicularis*) facility in this study. All experimental protocols were approved in advance by the Institutional Animal Care and Use Committee of Yunnan Key Laboratory of Primate Biomedical Research. The macaques were housed in a controlled environment (temperature: $22 \pm 1^\circ\text{C}$; humidity: $50\% \pm 5\%$ RH) with 12 hr light / 12 hr dark cycle (lights on at 08:00 a.m.). All macaques were given a commercial monkey diet twice a day with tap water ad libitum and were fed fruits and vegetables once daily. During and after experiments, macaques have been under careful veterinary oversight to ensure good health. In this study, a total of 39 cynomolgus macaques underwent MR scanning. These animals were scanned longitudinally during infancy and the adolescent period (from 1 month through 48 months of age, 23 females and 23 males),

Table 1
Recent available population-based macaque brain volumetric atlases.

Template	Species	Age	T1w /T2w	Age-specific or not	Subjects	Segmentation/ Probability for tissue	Parcellation
ONPRC18 (Weiss et al., 2020)	Rhesus (<i>M. mulatta</i>)	6–13 years	Both	Not	18 subjects	N/A	Cortical (36 ROIs) Subcortical (21 ROIs)
ONPRC Infant (Liu et al., 2019)	Rhesus (<i>M. mulatta</i>)	2, 4, 6 months	Both	2, 4, 6 months	6 subjects	Segmentation	INIA19 NeuroMaps (Rohlfing et al., 2012)
NMT V1.2 (Seidlitz et al., 2018)	Rhesus (<i>M. mulatta</i>)	3.2–13.2 years	T1w	Not	31 subjects	Segmentation	D99 parcellation (Reveley et al., 2016)
NMT V2.0 (Jung et al., 2020)	Rhesus (<i>M. mulatta</i>)	3.2–13.2 years	T1w	Not	31 subjects	Segmentation	Cortical (139 ROIs) Subcortical (210 ROIs)
UNC-Emory Infant (Shi et al., 2017)	Rhesus (<i>M. mulatta</i>)	2 weeks; 3, 6, 12 months	Both	2 weeks; 3, 6, 12 months	190 scans from 40 subjects	Probability	Lobar (16 ROIs) Subcortical (5 ROIs)
Lv et al. (Lv et al., 2020)	Cynomolgus (<i>M. fascicularis</i>)	3.5±1.8 years	T1w	Not	162 scans	Probability	D99 parcellation (Reveley et al., 2016)
Ours	Cynomolgus (<i>M. fascicularis</i>)	1, 2, 3, 4, 5, 6, 9, 12, 18, 24, 36, 48 months	Both	1, 2, 3, 4, 5, 6, 9, 12, 18, 24, 36, 48 months	175 scans from 39 subjects	Probability	Cortical (139 ROIs) Subcortical (210 ROIs) for each age-point

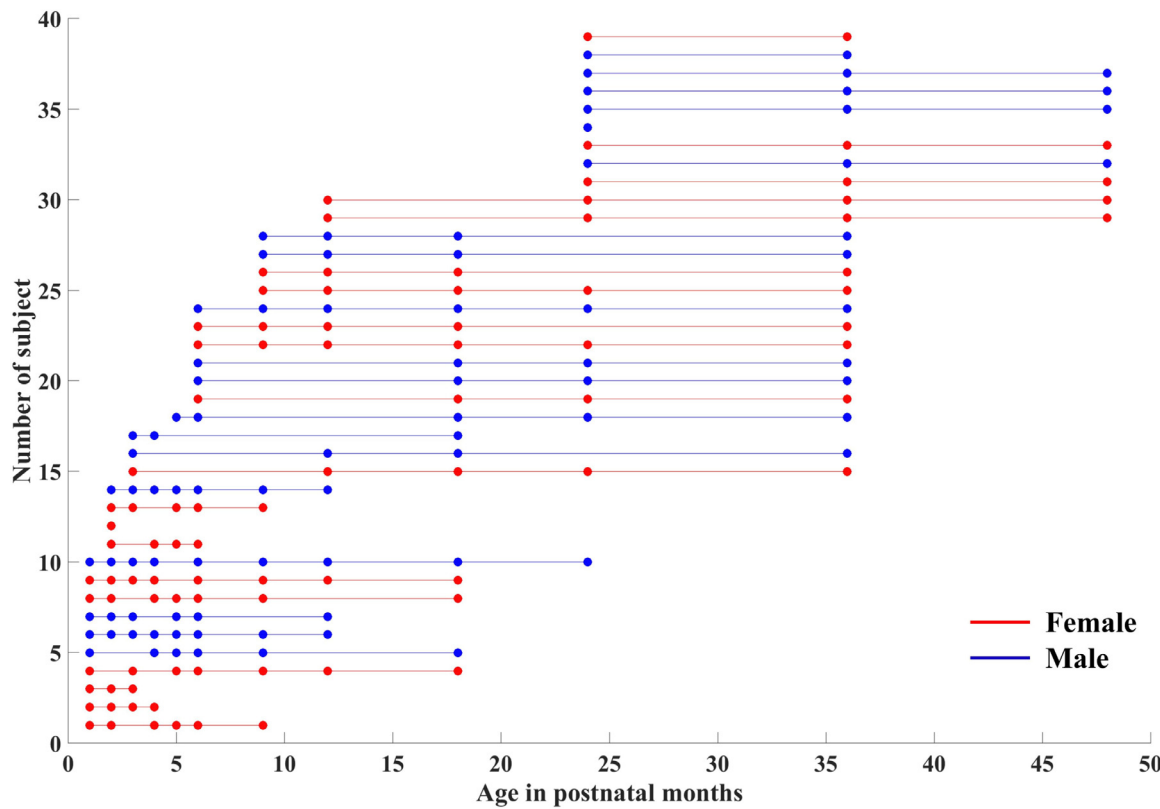


Fig. 2. The scan age and gender distributions for all subjects.

and a total of 175 scans were collected for the atlas construction. The age and gender distributions within each age group are shown in Fig. 2.

2.2. MRI acquisition

T1-weighted (T1w) and T2-weighted (T2w) images were acquired longitudinally at each time point (i.e., 1, 2, 3, 4, 5, 6, 9, 12, 18, 24, 36, and 48 months) by a GE Signa HDxT 3.0T MRI scanner. The T1w images were acquired with the following parameters: TR/TE = 5.836/2.020 ms, matrix = 256 × 256, in-plane resolution = 0.4688 × 0.4688 mm², slice thickness = 1.0 mm, spacing between slices = 0.5 mm. The T2w images were collected with the following parameters: TR/TE = 3000/100.725 ms, matrix = 256 × 256, in-plane resolution = 0.4688 × 0.4688 mm², slice thickness = 1.0 mm, spacing between slices = 0.5 mm.

2.3. Structural MRI atlas construction

The main steps in the atlas construction process, including image processing, atlases building, tissue probability maps creation, and parcellation maps generation, are shown in Fig. 3.

Image processing. All pairs of T1w and T2w images have undergone visual inspection to exclude images with substantial structural abnormalities and head motion. After initial quality control, N4 bias correction (Tustison et al., 2010) in ANTS (version 2.1; <http://stnava.github.io/ANTs/>) was used to perform initial image inhomogeneity correction. FMRIB's Linear Image Registration Tool (FLIRT) in FSL (version 5.0; <http://www.fmrib.ox.ac.uk/fsl/>) (Jenkinson et al., 2002; 2012) was used to rigidly align each T2w image to its corresponding T1w image, followed by being resampled to 0.5 mm isotropic resolution. All the T1w images were fed into the DIKA-Nets (Zhong et al.; 2021) for the macaque-dedicated skull stripping. The automatically generated brain masks were quality controlled and corrected by using ITK-snap software (Yushkevich et al., 2006) and then applied to the T2w images to obtain skull stripped T2w images. Then, we adopted

LINKS (Wang et al., 2015) to obtain the initial tissue segmentation map (including gray matter (GM), white matter (WM), and cerebrospinal fluid (CSF)) for each scan. LINKS is an in-house developed learning-based multi-source integration framework for brain tissue segmentation, which has been validated on MICCAI Neonatal Brain Segmentation (NeoBrainS12, <https://neobrainss12.isi.uu.nl/>) and 6-month infant brain MRI Segmentation (iSeg-2017, <https://iseg2017.web.unc.edu/>) Grand Challenges, achieving state-of-the-art performance. It leveraged random forest technique to effectively integrate features from multi-source images, i.e., initial T1w and T2w images and subsequently iteratively estimated and refined tissue probability maps of GM, WM, and CSF. Finally, the achieved segmentations were further manually corrected by experienced experts using ITK-Snap software (Yushkevich et al., 2006).

Atlases building. All images, including T1w, T2w, and tissue maps, were linearly aligned onto the UNC-Wisconsin juvenile macaque atlas (Styner et al., 2007) for initialization. Volumetric population-average atlases were independently generated at each time point (i.e., 1, 2, 3, 4, 5, 6, 9, 12, 18, 24, 36, and 48 months) based on both the intensity images and the corresponding tissue segmentation maps. To create an optimal population-averaged template in a diffeomorphic space, we employed the state-of-the-art symmetric group-wise normalization (SyGN) template building algorithm (Avants et al., 2011; 2010; Dong et al., 2020; Seidlitz et al., 2018; Tustison and Avants, 2013) provided by ANTs. SyGN considers both shape and appearance that are unbiased toward any specific individual and does not require user input or prior information, which proceeds according to the well-validated ‘optimal shape’ methodology detailed in Avants et al. (2011). For each age group, it performs the nonlinear iterative process of deformation as follows:

1. Creating the initial template of each modality, including T1w, T2w, and the tissue probability maps of GM, WM, and CSF, by averaging all individual images in each modality, respectively.

2. Performing symmetric normalization (SyN) algorithm (Avants et al., 2008) in ANTs based on multimodal information to

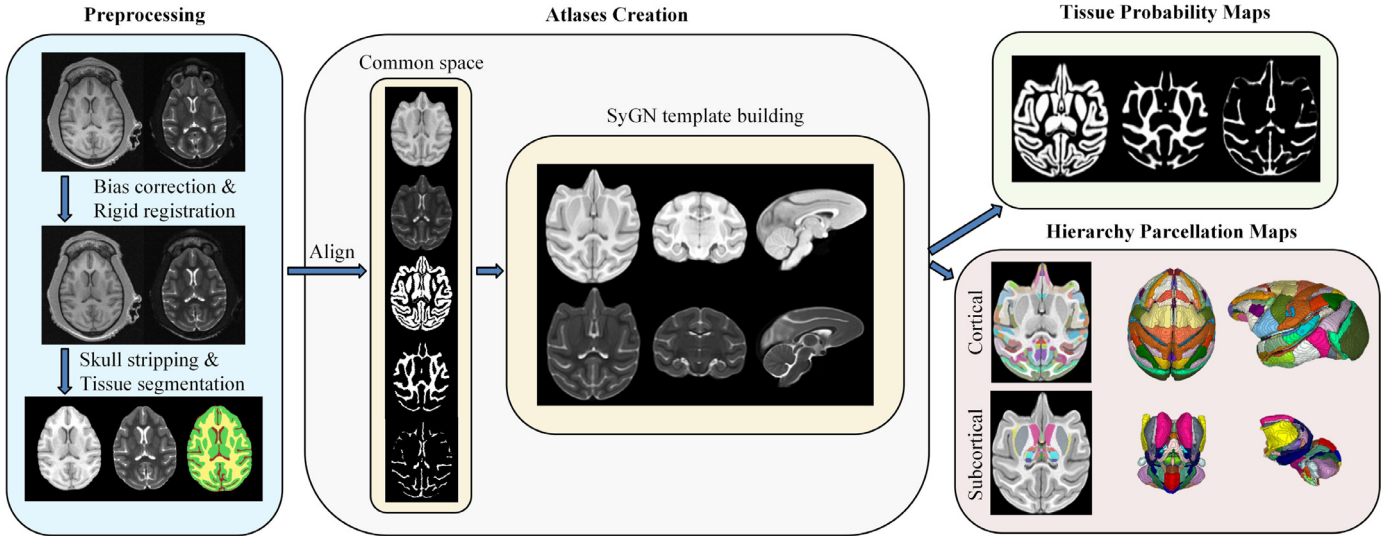


Fig. 3. The construction pipeline for each age-specific cynomolgus macaque brain atlas.

achieve pairwise registration from each individual image to the corresponding initial mean template. It is worth noting that SyN consisted of the consecutive transformations of rigid, affine, and diffeomorphic registration, which were combined as a single transform and applied to the original input images to minimize interpolation issues. Notably, different modalities will use the same transformation.

3. Applying gradient descent algorithm to maximize the appearance similarity metric between each individual image and its corresponding template to update the template appearance under a fixed template shape and mapping.

4. Optimizing the template shape. Specifically, the affine matrices and inverse deformation fields obtained in step 2 were averaged and then applied to each modality template obtained in step 3.

5. Using the updated multi-modal templates obtained in step 4 as the new initial templates in step 1 for the next iteration.

Considering that the SyGN algorithm usually converges after 3–5 iterations (Avants et al., 2010), we set the number of iterations to 5 for all age groups. Greedy B-spline SyGN was chosen as the transformation model (Tustison and Avants, 2013), and cross-correlation was the similarity metric for the brain registration, with SyGN default shrinkage factors, smoothing factors, and max iterations of $8 \times 4 \times 2 \times 1$, $3 \times 2 \times 1 \times 0$, and $100 \times 70 \times 50 \times 10$, respectively.

Tissue probability maps creation. Based on the previously obtained tissue segmentation maps of each scan, we respectively generated the tissue probability maps of WM, GM, and CSF for each age-specific atlas. These tissue probability maps can be used as prior maps by most tissue segmentation tools, such as AutoSeg (Wang et al., 2014), ANTS (Avants et al., 2011), and FSL (Jenkinson et al., 2012). The deformation field (nonlinear) and affine matrix (linear) of each subject, which were obtained in *Atlases creation* during each iteration, were combined and applied to the individual tissue segmentation maps. By doing this, all individual tissue segmentation maps were propagated to their corresponding age-specific atlas. These warped maps were then averaged across individuals in terms of each tissue type to produce mean WM, GM, and CSF tissue probability maps for each age-specific atlas.

Parcellation maps generation. To obtain the parcellation maps of the generated cynomolgus atlases, we used the SyN algorithm to warp the NMT v2 template (Hartig et al., 2020; Jung et al., 2020) to the current template space, and then applied the diffeomorphic transformation to the Cortical Hierarchy Atlas of the Rhesus Macaque (CHARM) and Subcortical Hierarchy Atlas of the Rhesus Macaque (SHARM), which are the parcellation maps provided by the NMT v2 atlas. Considering the continuous developmental changes between adjacent age points are

much smaller than that between adults and neonates, we performed an age-continuous propagation strategy instead of direct propagation from adult to neonatal brains, which typically leads to longitudinal inconsistency and large errors of the parcellation maps due to the direct independent propagation for each early age, as shown in Fig. 4. Specifically, we first warped the NMT v2 T1w template to our generated 48-months T1w template to obtain the deformation field. Then, we sequentially warped the older template to the younger template between each two adjacent age points to generate the corresponding deformation field. Finally, we concatenated related deformation fields as a single diffeomorphic transform and used it to propagate the CHARM and SHARM parcellation maps to each age-specific atlas. Using the same strategy, the ventricle mask from NMT v2 was also propagated to each age-specific atlas.

3. Results

3.1. Longitudinal cynomolgus macaque templates

All atlas files are generated in NIFTI (Neuroimaging Informatics Technology Initiative) file format with a grid size of $320 \times 320 \times 150$ pixels and 0.38 mm isotropic pixel size. Twelve unbiased age-specific templates densely covering from 1 to 48 months development period were successfully created using the procedures outlined in Section 2.3. Typical axial slices from the longitudinal age-specific cynomolgus macaque templates are shown in Fig. 5, together with the tissue probability maps for GM, WM, and CSF. Note that these templates show dynamic neurodevelopment in brain appearances and anatomical structures, especially in the first year. Each voxel in the tissue probability map contains a value between 0 and 1, describing the average likelihood that the voxel belongs to a specific tissue type. To better display the high quality of the created atlases, we show five axial slices (from bottom to top) of T1w images, T2w images, and corresponding tissue probability maps at 12-months in Fig. 6. From these figures, we can see that the generated tissue probability maps precisely match each tissue in template images, revealing apparent age-specific anatomical structures.

3.2. Longitudinal hierarchical parcellation maps

Parcellation for regions of interest (ROIs) was generated by nonlinearly aligning the NMT v2 template to our templates to propagate the CHARM and SHARM label maps to each age-specific atlas. The CHARM and SHARM label maps describe the anatomical makeup of the cortical

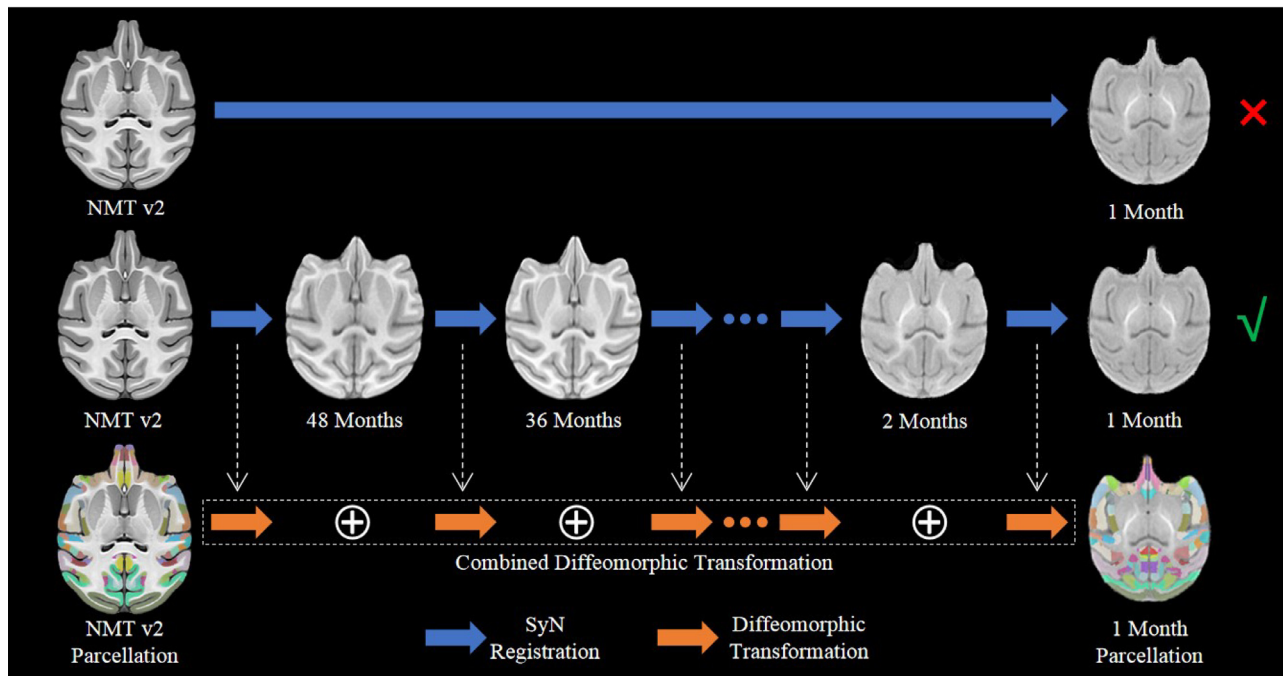


Fig. 4. An example overview of age-continuous parcellation propagation from NMT v2 template to the generated 1-month template. Corresponding diffeomorphic transformations generated by SyN registration between adjacent age points were combined as a single transformation for each age and applied to the NMT v2 parcellation to obtain each age-specific parcellation.

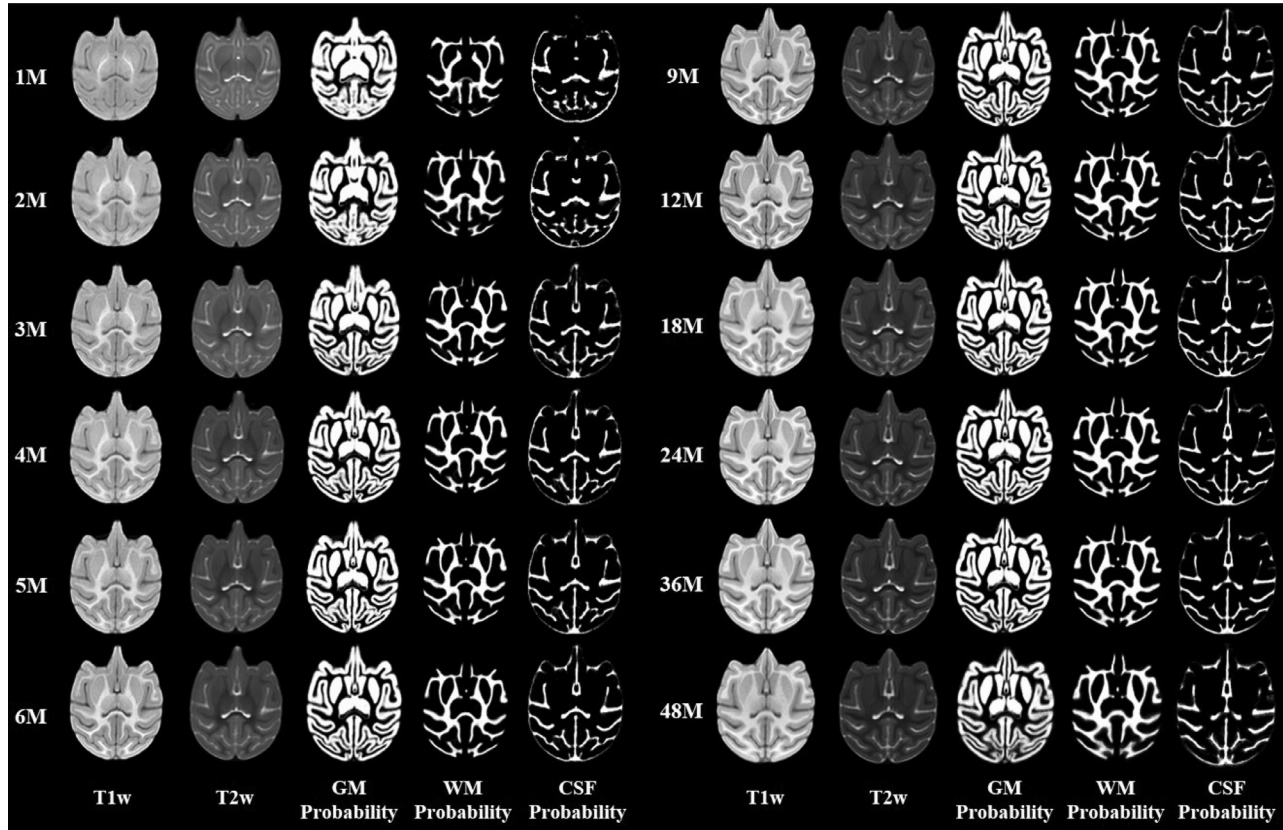


Fig. 5. The constructed longitudinal cynomolgus macaque brain templates from 1 to 48 months of age. The ages in months are indicated on the left.

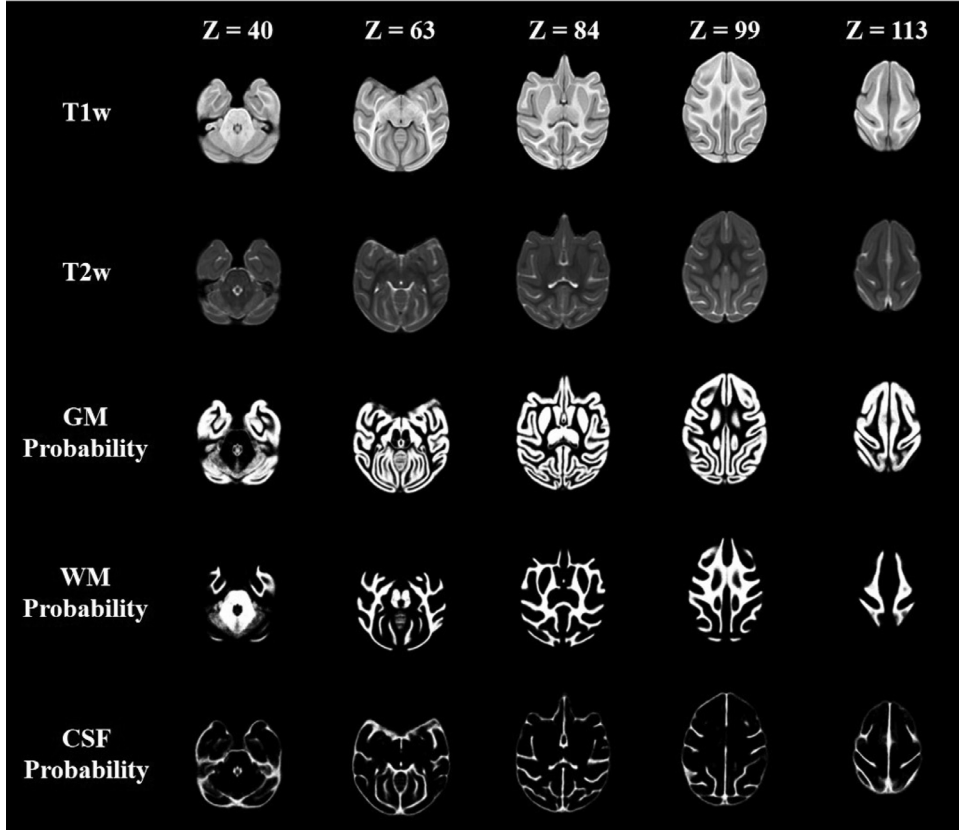


Fig. 6. Templates and corresponding tissue probability maps of 12-month cynomolgus macaques. Five axial slices from T1w images, T2w images, the gray matter (GM, third row), white matter (WM, fourth row), and cerebrospinal fluid (CSF, fifth row) are illustrated.

and subcortical regions at different spatial scales (a total of 6 levels), as shown in Fig. 7. Individual ROIs at level 6 were grouped into progressively larger groups from level 5 to level 1. Each ROI or group of ROIs at a lower level (e.g., level 6) belongs to exactly one group in the next higher level (e.g., level 5). The broadest scale (level 1) of CHARM contains the four cortical lobes, which are iteratively subdivided until the finest scale (level 6, 139 ROIs) in the subsequent levels. The broadest scale (level 1) of SHARM assembles all ROIs of subcortical structures, according to the classical developmental division of the neuraxis, into five regions, namely the (subcortical) telencephalon, diencephalon, mesencephalon, metencephalon, and myelencephalon. As the broadest scale level increases, the ROIs are continually subdivided until the finest scale (level 6, 210 ROIs) based on different degrees of anatomical details and functional relationships. Consequently, the brain template of each age group has corresponding propagated CHARM and SHARM label maps, and thus can provide various levels of parcellation maps suitable for different ROI-based analyses within each specific age group.

3.3. Developmental trajectories of brain structures

Based on our longitudinal cynomolgus macaque dataset, we estimated the developmental trajectories of brain structures to analyze the postnatal brain changes quantitatively. Specifically, we measured the total brain volume (TBV), white matter volume (WMV) and gray matter volume (GMV), and generated developmental trajectories for males and females independently to show gender differences. We applied a nonparametric regression method, i.e., generalized additive mixed models (GAMM) (Lin and Zhang, 1999), to deal with the nonlinear and dynamic nature of early brain development. Let $v_i(t)$ denote the brain structure volume for the i^{th} subject at the postnatal age t , the GAMM can be defined as: $v_i(t) = f(t) + \Delta(t) * g_i + \alpha_i + e_i(t)$. where $g_i = 1$ if the gender

is male and 0 otherwise; α_i is the random intercept effect; $e_i(t)$ is the random Gaussian noise. With these variables described above, cubic splines were applied to obtain the estimated nonparametric functions $v_i(t)$ and $\Delta(t)$. Besides, to identify the age ranges with significant gender differences, we used the Bayesian posterior covariance matrix (Lin and Zhang, 1999) to generate 95% confidence intervals of the fixed effect for both genders. All steps above were performed with the R package itsadug (Sóskuthy, 2017).

As shown in Fig. 8, the most rapid postnatal growth of each structure occurs at the age before 6 months, indicating the necessity of construction of temporally dense atlases during this early postnatal stage. Specifically, from 1 to 6 months, the growth rate of TBV/WMV/GMV is 22.81%/26.33%/10.77% for females and 26.12%/30.37%/13.42% for males, respectively; while from 1 to 12 months, the growth rate of TBV/WMV/GMV is 26.08%/38.01%/10.15% for females and 32.32%/45.81%/15.27% for males, respectively. From 1 to 24 months of age, the growth rate of TBV/WMV/GMV is 31.82%/44.75%/15.07% for females and 42.33%/58.48%/23.42% for males, respectively. From 1 to 48 months of age, the growth rate of TBV/WMV/GMV is 31.39%/48.41%/13.22% for females and 44.01%/67.72%/22.75% for males, respectively. It can be seen that the dynamic postnatal brain volume increase is contributed more by the increase in WMV, compared to GMV. From 24 to 48 months of age, the growth rate of TBV/WMV/GMV is -0.32%/2.53%/-1.60% for females and 1.18%/5.84%/-0.55% for males, respectively. During this period, WMV for both genders showed a stable growth as age advanced, while GMV for both genders decreased. Noticeable gender differences in volume begin to present at around 12 months, i.e., all volumes of males are larger than those of females, with statistically significant differences presented after 36 months for TBV and WMV. These estimated trajectories suggest that the early postnatal brain development of cynomolgus macaques largely resembles the pre-

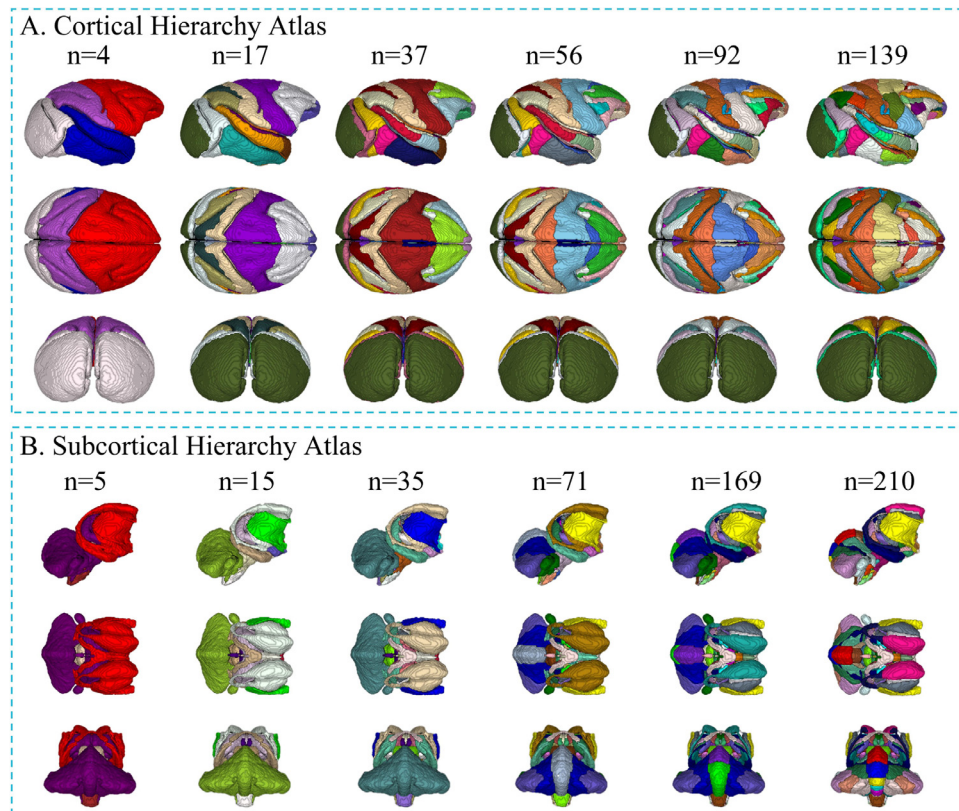


Fig. 7. 3D rendering of the generated parcelation maps at 12-month age point (along with the number ‘n’ of regions at each level). As the level increases from left to right (level 1 to level 6), the cortical and subcortical structures are continuously subdivided into smaller regions based on anatomical landmarks, functional relationships, and cytoarchitectonics. (A) 3D-rendering of Cortical Hierarchy Atlas. (B) 3D-rendering of Subcortical Hierarchy Atlas.

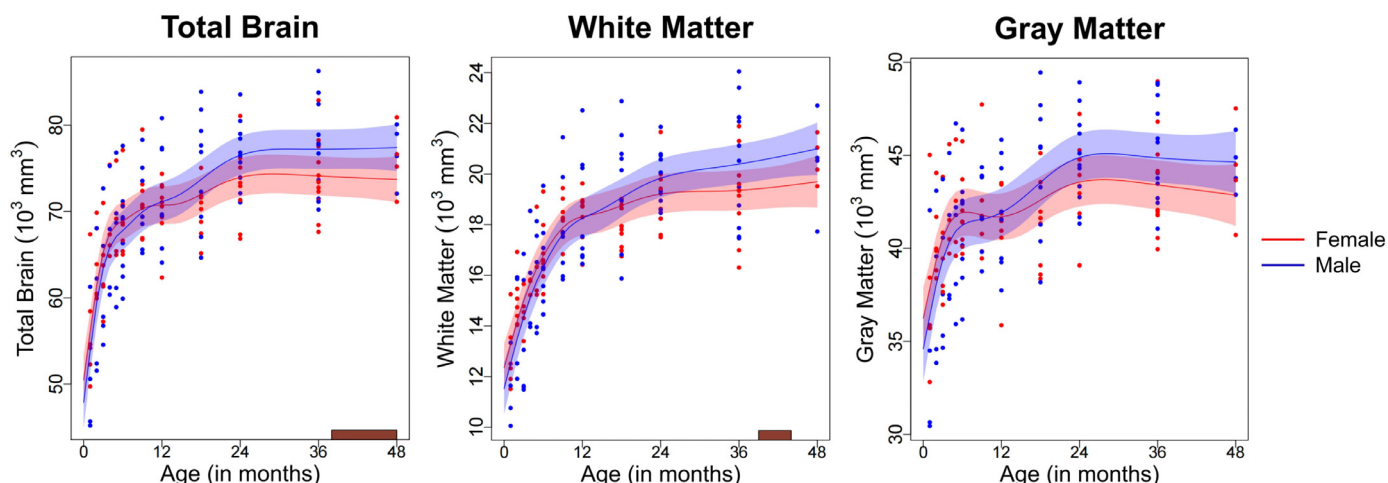


Fig. 8. Growth trajectories of the total brain volume, white matter volume, and gray matter volume for female (red) and male (blue) subjects from 1 to 48 months of age. Age ranges of significant gender difference with 95% confidence intervals were included on the x-axis as dark red segments. (For interpretation of the references to colour in this figure legend, the reader is referred to the web version of this article.)

vious findings of both human and rhesus macaque brain development studies (Ball and Seal, 2019; Knickmeyer et al., 2010; Scott et al., 2016; Sussman et al., 2016).

4. Discussion

In this study, we used 175 longitudinal brain MRI scans of naturally reared cynomolgus macaques to construct the most comprehensive developing brain atlases to date. To this end, a total of 39 brains (20 females and 19 males) were longitudinally scanned. Six time points during the first half year of life and nine time points during the first year

of life provided the most temporal dense profiles of the early postnatal brain development.

4.1. Longitudinal age-specific brain atlases for cynomolgus macaques

A variety of rhesus macaque atlases are currently available, including those based on an individual animal, such as the F99 atlas (Van Essen, 2004) and 3D digital D99 atlas (Reveley et al., 2016), or based on multiple subjects, such as 112RM-SL (McLaren et al., 2009), MNI Institute (Frey et al., 2011), INIA19 (Rohlfing et al., 2012), UNC-Emory Infant Rhesus Atlases (Shi et al., 2017), and NMT v1 atlas (Seidlitz et al., 2018). Studies have shown differences in the brain struc-

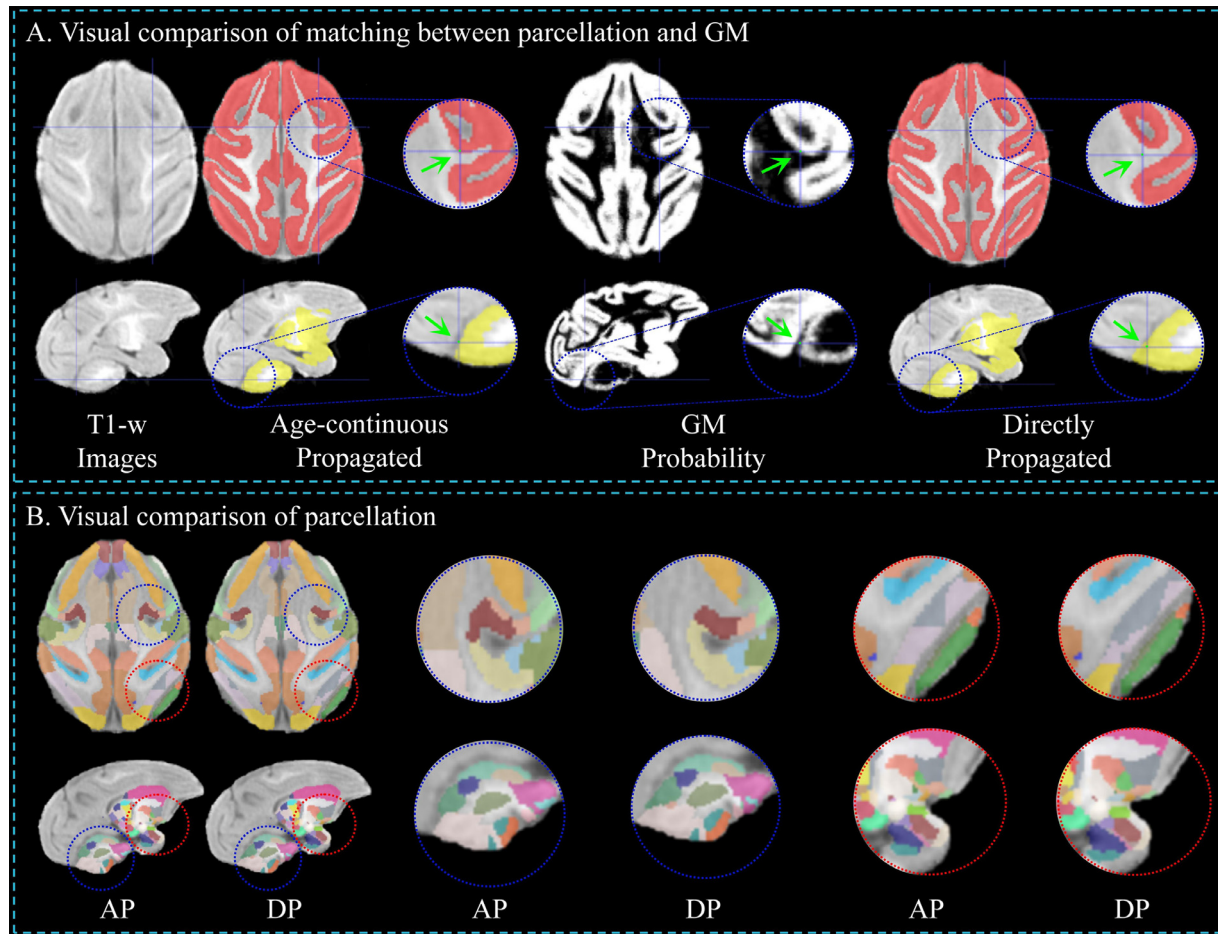


Fig. 9. Visual comparison of parcellation maps of 1-month template obtained by different methods. (A) Visual comparison of matching between parcellation and GM probability map. Blue crosses locate the same position in each map in the unified anatomical space, highlighted by green arrows and points. Red masks represent the cerebral cortex, while the yellow masks represent the subcortical and cerebellar areas. (B) Visual comparison of age-continuous propagation (AP) and direct propagation (DP) based parcellations. (For interpretation of the references to colour in this figure legend, the reader is referred to the web version of this article.)

tures between rhesus and cynomolgus macaques, e.g., sulcal patterns (Van Essen, 2004), brain volume (McLaren et al., 2009), and skull shape (Frey et al., 2011). Recently, a population-based cynomolgus macaque atlas, based on subjects with age ranging between 2 and 9 years, was available (Lv et al., 2020). However, this atlas cannot characterize the early postnatal brain development of macaques, which is a dynamic and regionally heterogeneous complex process for brain structures (Scott et al., 2016). Meanwhile, many human neuroscience studies have proved that applying adult-based atlases as a reference to normalize MR images of infant brains is less accurate than using infant dedicated atlases (Fillmore et al., 2015; Fonov et al., 2011; Sanchez et al., 2012; Yoon et al., 2009). Moreover, volumetric image registration accuracy is significantly improved by performing the spatial normalization with an age-matching template (Shen et al., 2007). Due to the remarkable inter-species and inter-age variability, it is expected that future studies on non-human primates, especially quantitative analysis, will benefit from the brain atlases of specific species with densely sampled time points during infancy.

Therefore, this study aimed to construct densely-sampled cynomolgus macaque brain MRI atlases during early postnatal development. These atlases were constructed from 175 high-quality MRI scans, including T1-weighted and T2-weighted images, of cynomolgus monkeys with age ranging from 1 to 48 months. Each resulting age-specific brain atlas comprises volumetric brain templates (T1w and T2w images), tissue probability maps, and hierarchy parcellation maps. Such a large

longitudinal cynomolgus brain dataset ensures that the constructed 4D atlases can encapsulate the intra-species and developmental changes in cynomolgus brains. The widely-validated state-of-the-art SyGN template building algorithm (Avants et al., 2011; 2010) was employed to couple a large sample of individuals together to build unbiased high-quality brain templates. The GM, WM, and CSF tissue probability maps of the cynomolgus brain at each age level were also created based on manually-checked tissue segmentation maps. The atlases provide a common coordinate space for cynomolgus macaques, which can greatly help perform related voxel-based analyses, e.g., brain tissue segmentation, regions of interest delineation, and visualizing data collected across ages and sites. Furthermore, these 4D atlases can help precisely warp individual subjects to their corresponding age-level template and accurately locate brain regions, which is critical for making experimental plans for anatomical tracer injection, surgical injury, or electrophysiological penetration.

In order to generate high-quality parcellation maps for our 4D atlases, the accurate nonlinear transformation from the source atlas (NMT v2, based on adults) to the target atlas (generated longitudinal cynomolgus atlas) is highly required. However, supposing we directly transform the source adults NMT atlas to target neonatal atlas, the neonatal brain's distinct appearance, shape and low-contrast may significantly degrade the registration accuracy, making the generated parcels unable to match the brain template well. Taking advantage of our datasets with densely sampled time-points, we constructed corresponding brain atlases with

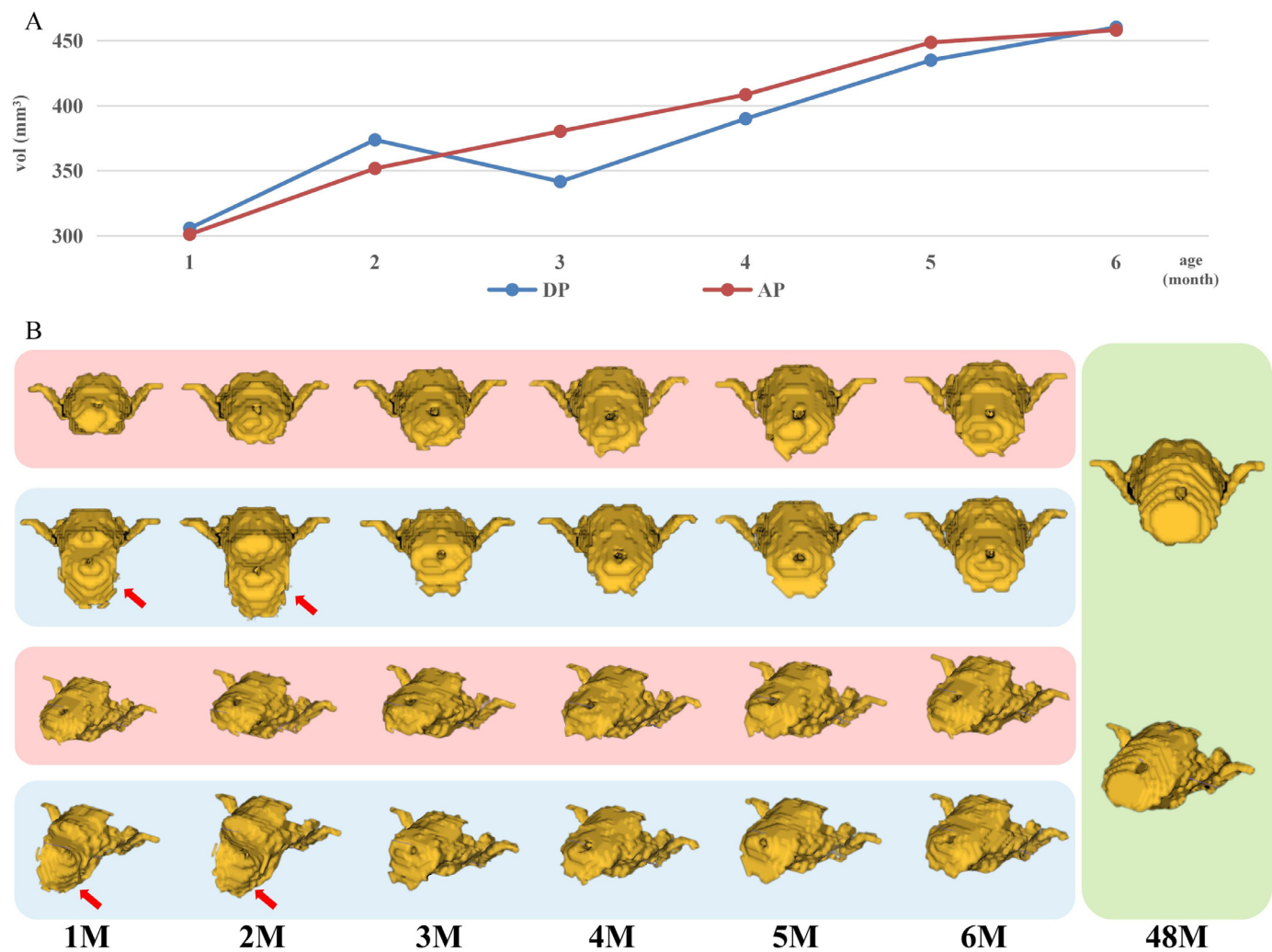


Fig. 10. Volume changes and surface rendering of the myelencephalon from 1 to 6 months. (A) shows the volume developmental trajectories; (B) shows the surface rendering results. Results of the age-continuous propagation (AP, in red boxes) and the direct propagation (DP, in blue boxes) in two different views are shown. The surface rendering results of 48-months are also shown in green box for better comparison. (For interpretation of the references to colour in this figure legend, the reader is referred to the web version of this article.)

continuous age points at the early developmental period after birth. Considering the continuous developmental changes between adjacent age points are smaller than that between adult and neonatal brains, we perform continuous propagation from each older age to its younger adjacent age, instead of direct transformation from adult brains to neonatal brains, to better match the anatomical structures of brain templates. As shown in Fig. 9 (A), both cortical area (red) and non-cortical area (yellow) achieved by age-continuous propagation match the GM probability map better than the results obtained by direct propagation. This difference can be visually observed from the position located by the blue cross. Specifically, the point is located at the boundary in the results of age-continuous propagation and GM probability map, while located far away from the boundary in the results of direct propagation. Besides, the parcellations generated by the two different methods also show a notable difference in the size and shape of each ROI, as shown in Fig. 9 (B). Although there is no ground truth of parcellation for generated atlases, the age-continuous propagation based parcellation should be more accurate than the direct propagation based parcellation, which is confirmed by Fig. 9 (A). These results also indicate the necessity of the proposed age-continuous propagation strategy and the importance of the temporally densely sampled atlases.

For a better comparison of the two propagation strategies, we provided volume changes and 3D surface renderings of Myelencephalon (or medulla) as an example. The myelencephalon is the posterior por-

tion of the brain stem, which is composed largely of tracts carrying signals between the rest of the brain and the body. Since the macaque brain develops rapidly in the first six months, we show the trajectories of volume and surface renderings of the myelencephalon during this stage. As shown in Fig. 10, the age-continuous propagation results lead to monotone and longitudinally-consistent increasing of the myelencephalon volume during brain development, while the direct propagation results show non-monotone increasing, which is clearly less realistic. Meanwhile, the surface rendering results of the age-continuous propagation better preserve the shape of the myelencephalon in longitudinal atlases than those of the direct propagation, as shown in the bottom part of Fig. 10. The noisy results of the direct propagation are caused by the inaccurate and longitudinally inconsistent registration, due to the large intensity and anatomical differences between the early-month images and the adult images. Hence, the age-continuous propagation used in our constructed atlas can generate more accurate and consistent parcellation maps, thus better representing the shape consistency and developmental trajectories.

4.2. Limitations and future directions

The 3D NMT v2 macaque brain atlas 6-level hierarchy parcellation maps, including Cortical Hierarchy Atlas and Subcortical Hierarchy Atlases (Hartig et al., 2020; Jung et al., 2020) are used to generate par-

cellation maps for our constructed atlases, thus providing comprehensive and hierarchical cortical and subcortical regions. However, this parcellation is created based on rhesus macaques rather than cynomolgus macaques. Though both species are from the genus Macaca and show patterns of allele sharing across the species boundary (Carlsson et al., 2004; Satkoski Trask et al., 2013; Yan et al., 2011), differences in their brain structures have been reported (Frey et al., 2011; Van der Gucht et al., 2006; McLaren et al., 2009). Applying the rhesus macaque labelmap to the cynomolgus macaque atlases would be an acceptable solution (Lv et al., 2020), due to the lack of alternatives. Therefore, there is still a lack of a high-resolution parcellation scheme specific to cynomolgus macaques.

Besides volumetric atlases, the benefits of providing surface-based atlases have been highlighted by some researches (Van Essen and Dierker, 2007; Li et al., 2015; Wang, Lian, Xia, Wu, Duan, Wang, Shen, Li; Wu et al., 2019; Xia et al., 2019). The 4D surface-based cynomolgus brain atlases could contribute valuable and accurate references for brain studies by respecting the topology of the highly convoluted cerebral cortex. Furthermore, a complementary longitudinal diffusion tensor cynomolgus brain atlas would promote the studies of cynomolgus cortical microstructure and white matter organization (Adluru et al., 2012; Kroenke et al., 2007). Therefore, our future work would focus on creating the 4D surface-based and diffusion tensor-based cynomolgus brain atlases.

5. Conclusion

We constructed a set of longitudinal early developing cynomolgus macaque brain atlases associated with anatomical information, including tissue probability maps and hierarchy parcellation maps. These atlases provide, to our knowledge, the most temporally dense templates for the dynamic features of monkey brain during the early postnatal development, especially the first year of life. These longitudinal brain atlases will greatly benefit the neuroscience community in biomedical studies of non-human primates and ultimately deep our understanding on structure-function relationship in human brains in early critical development. The generated longitudinal cynomolgus macaque atlases will be publicly available on the website of Yunnan key laboratory of primate biomedical research (www.lpbr.cn) and NITRC (https://www.nitrc.org/projects/cyno_4d_atlas/) website to greatly facilitate early brain development studies.

Data availability statement

The cynomolgus macaques data that support the findings of this study are available from [Yunnan Key Laboratory of Primate Biomedical Research, Institute of Primate Translational Medicine, Kunming University of Science and Technology, Kunming, China], but restrictions apply to the availability of these data, which were used under license for the current study, and thus they are not publicly available. Data are however available from the authors upon reasonable request and with permission of [Yunnan Key Laboratory of Primate Biomedical Research]. AAALAC International accredits the cynomolgus macaque (*Macaca fascicularis*) facility in this study. All experimental protocols were approved in advance by the Institutional Animal Care and Use Committee of Yunnan Key Laboratory of Primate Biomedical Research.

CRediT authorship contribution statement

Tao Zhong: Writing – original draft, Writing – review & editing, Methodology, Software. **Jingkuan Wei:** Data acquisition and collection. **Kunhua Wu:** Data acquisition and collection. **Liangjun Chen:** Writing – review & editing, Software. **Fenqiang Zhao:** Writing – review & editing. **Yuchen Pei:** Data curation. **Ya Wang:** Data curation. **Hongjiang Zhang:** Data collection. **Zhengwang Wu:** Writing – review & editing. **Ying Huang:** Formal analysis. **Tengfei Li:** Formal analysis. **Li Wang:**

Data curation. **Yongchang Chen:** Data collection. **Weizhi Ji:** Data collection. **Yu Zhang:** Supervision. **Gang Li:** Conceptualization, Supervision, Writing – review & editing, Methodology. **Yuyu Niu:** Data acquisition and collection, Writing – review & editing.

Acknowledgments

This study was partially supported by grants from the National Natural Science Foundation of China [grant number: 32070541 to Y N], and the Natural Science Foundation of Yunnan [grant number: 202001BC070001 to W J, 202101AT070278 to J W].

References

- Adluru, N., Zhang, H., Fox, A.S., Shelton, S.E., Ennis, C.M., Bartosic, A.M., Oler, J.A., Tromp, D.P., Zakszewski, E., Gee, J.C., 2012. A diffusion tensor brain template for rhesus macaques. *Neuroimage* 59, 306–318.
- Avants, B.B., Epstein, C.L., Grossman, M., Gee, J.C., 2008. Symmetric diffeomorphic image registration with cross-correlation: evaluating automated labeling of elderly and neurodegenerative brain. *Med. Image Anal.* 12, 26–41.
- Avants, B.B., Tustison, N.J., Song, G., Cook, P.A., Klein, A., Gee, J.C., 2011. A reproducible evaluation of ants similarity metric performance in brain image registration. *Neuroimage* 54, 2033–2044.
- Avants, B.B., Yushkevich, P., Pluta, J., Minkoff, D., Korczykowski, M., Detre, J., Gee, J.C., 2010. The optimal template effect in hippocampus studies of diseased populations. *Neuroimage* 49, 2457–2466.
- Ball, G., Seal, M.L., 2019. Individual variation in longitudinal postnatal development of the primate brain. *Brain Struct. Funct.* 224, 1185–1201.
- Belmonte, J.C.I., Callaway, E.M., Caddick, S.J., Churchland, P., Feng, G., Homanics, G.E., Lee, K.F., Leopold, D.A., Miller, C.T., Mitchell, J.F., 2015. Brains, genes, and primates. *Neuron* 86, 617–631.
- Capitanio, J.P., Emborg, M.E., 2008. Contributions of non-human primates to neuroscience research. *Lancet* 371, 1126–1135.
- Carlsson, H., Schapiro, S.J., Farah, I., Hau, J., 2004. Use of primates in research: a global overview. *Am. J. Primatol. Off. J. Am. Soc. Primatol.* 63, 225–237.
- Chen, Y., Yu, J., Niu, Y., Qin, D., Liu, H., Li, G., Hu, Y., Wang, J., Lu, Y., Kang, Y., 2017. Modeling Rett syndrome using TALEN-edited MECP2 mutant cynomolgus monkeys. *Cell* 169, 945–955.e10.
- Dong, H.M., Castellanos, F.X., Yang, N., Zhang, Z., Zhou, Q., He, Y., Zhang, L., Xu, T., Holmes, A.J., Yeo, B.T., et al., 2020. Charting brain growth in tandem with brain templates at school age. *Sci. Bull.* 65, 1924–1934.
- Fillmore, P.T., Phillips-Meek, M.C., Richards, J.E., 2015. Age-specific MRI brain and head templates for healthy adults from 20 through 89 years of age. *Front. Aging Neurosci.* 7, 44.
- Fonov, V., Evans, A.C., Botteron, K., Almlie, C.R., McKinstry, R.C., Collins, D.L., Group, B.D.C., 2011. Unbiased average age-appropriate atlases for pediatric studies. *Neuroimage* 54, 313–327.
- Frey, S., Pandya, D.N., Chakravarty, M.M., Bailey, L., Petrides, M., Collins, D.L., 2011. An MRI based average macaque monkey stereotaxic atlas and space (MNI monkey space). *Neuroimage* 55, 1435–1442.
- Friston, K.J., Holmes, A.P., Price, C., Böchel, C., Worsley, K., 1999. Multisubject fmri studies and conjunction analyses. *Neuroimage* 10, 385–396.
- Van der Gucht, E., Youakim, M., Arckens, L., Hof, P.R., Baizer, J.S., 2006. Variations in the structure of the prelunate gyrus in old world monkeys. *Anat. Rec. Part A Discov. Mol. Cell. Evolut. Biol. Off. Publ. Am. Assoc. Anat.* 288, 753–775.
- Hartig, R., Glen, D., Jung, B., Logothetis, N. K., Paxinos, G., Garza-Villarreal, E. A., Messinger, A., Evrard, H. C., 2020. Subcortical atlas of the rhesus macaque (SARM) for magnetic resonance imaging. *BioRxiv*, 2020.09.16.300053 Doi: 10.1101/2020.09.16.300053.
- Holmes, C.J., Hoge, R., Collins, L., Woods, R., Toga, A.W., Evans, A.C., 1998. Enhancement of MR images using registration for signal averaging. *J. Comput. Assist. Tomogr.* 22, 324–333.
- Jenkinson, M., Barnister, P., Brady, M., Smith, S., 2002. Improved optimization for the robust and accurate linear registration and motion correction of brain images. *Neuroimage* 17, 825–841.
- Jenkinson, M., Beckmann, C.F., Behrens, T.E., Woolrich, M.W., Smith, S.M., 2012. Fsl. *Neuroimage* 62, 782–790.
- Jennings, C.G., Landman, R., Zhou, Y., Sharma, J., Hyman, J., Movshon, J.A., Qiu, Z., Roberts, A.C., Roe, A.W., Wang, X., 2016. Opportunities and challenges in modeling human brain disorders in transgenic primates. *Nat. Neurosci.* 19, 1123–1130.
- Jung, B., Taylor, P. A., Seiditz, J., Sponheim, C., Perkins, P., Ungerleider, L. G., Glen, D., Messinger, A., 2020. A comprehensive macaque fMRI pipeline and hierarchical atlas. *BioRxiv*, 2020.08.05.237818 Doi:10.1101/2020.08.05.237818.
- Knickmeyer, R.C., Gouttard, S., Kang, C., Evans, D., Wilber, K., Smith, J.K., Hamer, R.M., Lin, W., Gerig, G., Gilmore, J.H., 2008. A structural MRI study of human brain development from birth to 2 years. *J. Neurosci.* 28, 12176–12182.
- Knickmeyer, R.C., Styner, M., Short, S.J., Lubach, G.R., Kang, C., Hamer, R., Coe, C.L., Gilmore, J.H., 2010. Maturational trajectories of cortical brain development through the pubertal transition: unique species and sex differences in the monkey revealed through structural magnetic resonance imaging. *Cereb. Cortex* 20, 1053–1063.
- Kroenke, C.D., Van Essen, D.C., Inder, T.E., Rees, S., Brethorst, G.L., Neil, J.J., 2007. Microstructural changes of the baboon cerebral cortex during gestational develop-

- ment reflected in magnetic resonance imaging diffusion anisotropy. *J. Neurosci.* 27, 12506–12515.
- Li, G., Nie, J., Wang, L., Shi, F., Gilmore, J.H., Lin, W., Shen, D., 2014. Measuring the dynamic longitudinal cortex development in infants by reconstruction of temporally consistent cortical surfaces. *Neuroimage* 90, 266–279.
- Li, G., Wang, L., Shi, F., Gilmore, J.H., Lin, W., Shen, D., 2015. Construction of 4D high-definition cortical surface atlases of infants: Methods and applications. *Medical Image Analysis* doi:10.1016/j.media.2015.04.005.
- Li, G., Wang, L., Shi, F., Lyall, A.E., Lin, W., Gilmore, J.H., Shen, D., 2014. Mapping longitudinal development of local cortical gyration in infants from birth to 2 years of age. *Journal of Neuroscience* doi:10.1523/JNEUROSCI.3976-13.2014.
- Li, G., Wang, L., Yap, P.T., Wang, F., Wu, Z., Meng, Y., Dong, P., Kim, J., Shi, F., Rekik, I., 2019. Computational neuroanatomy of baby brains: a review. *Neuroimage* 185, 906–925.
- Lin, X., Zhang, D., 1999. Inference in generalized additive mixed models by using smoothing splines. *J. R. Stat. Soc. Ser. B (Stat. Methodol.)* 61, 381–400.
- Liu, Z., Li, X., Zhang, J.T., Cai, Y.J., Cheng, T.L., Cheng, C., Wang, Y., Zhang, C.C., Nie, Y.H., Chen, Z.F., 2016. Autism-like behaviours and germline transmission in transgenic monkeys overexpressing MECP2. *Nature* 530, 98–102.
- Liu, Z., Neuringer, M., Erdman, J.W., Kuchan, M.J., Renner, L., Johnson, E.E., Wang, X., Kroenke, C.D., 2019. The effects of breastfeeding versus formula-feeding on cerebral cortex maturation in infant rhesus macaques. *Neuroimage* 184, 372–385.
- Lv, Q., Yan, M., Shen, X., Wu, J., Yu, W., Yan, S., Yang, F., Zeljic, K., Shi, Y., Zhou, Z., Lv, L., Hu, X., Menon, R., Wang, Z., 2020. Normative analysis of individual brain differences based on a population MRI-based atlas of cynomolgus macaques. *Cereb. Cortex* doi:10.1093/cercor/bhaa229.
- Malkova, L., Heuer, E., Saunders, R., 2006. Longitudinal magnetic resonance imaging study of rhesus monkey brain development. *Eur. J. Neurosci.* 24, 3204–3212.
- Mazziotta, J., Toga, A., Evans, A., Fox, P., Lancaster, J., Zilles, K., Woods, R., Paus, T., Simpson, G., Pike, B., 2001. A probabilistic atlas and reference system for the human brain: international consortium for brain mapping (ICBM). *Philos. Trans. R. Soc. Lond. Ser. B Biol. Sci.* 356, 1293–1322.
- McLaren, D.G., Kosmatka, K.J., Oakes, T.R., Kroenke, C.D., Kohama, S.G., Matochik, J.A., Ingram, D.K., Johnson, S.C., 2009. A population-average MRI-based atlas collection of the rhesus macaque. *Neuroimage* 45, 52–59.
- Nie, J., Li, G., Shen, D., 2013. Development of cortical anatomical properties from early childhood to early adulthood. *Neuroimage* doi:10.1016/j.neuroimage.2013.03.021.
- Poo, M.m., Du, J.l., Ip, N.Y., Xiong, Z.Q., Xu, B., Tan, T., 2016. China brain project: basic neuroscience, brain diseases, and brain-inspired computing. *Neuron* 92, 591–596.
- Quollo, M., Price, C.J., Ueno, K., Asamizuya, T., Cheng, K., Lemon, R., Iriki, A., 2010. Creating a population-averaged standard brain template for Japanese macaques (m. fascicata). *Neuroimage* 52, 1328–1333.
- Reveley, C., Gruslys, A., Ye, F.Q., Glen, D., Samaha, J., E. Russ, B., Saad, Z., K. Seth, A., Leopold, D.A., Saleem, K.S., 2016. Three-dimensional digital template atlas of the macaque brain. *Cereb. Cortex* 27, 4463–4477. doi:10.1093/cercor/bhw248.
- Rilling, J.K., 2014. Comparative primate neurobiology and the evolution of brain language systems. *Curr. Opin. Neurobiol.* 28, 10–14.
- Rohlfing, T., Kroenke, C.D., Sullivan, E.V., Dubach, M.F., Bowden, D.M., Grant, K., Pfefferbaum, A., 2012. The inia19 template and neuromaps atlas for primate brain image parcellation and spatial normalization. *Front. Neuroinform.* 6, 27.
- Sanchez, C.E., Richards, J.E., Almli, C.R., 2012. Age-specific MRI templates for pediatric neuroimaging. *Dev. Neuropsychol.* 37, 379–399.
- Satkoski Trask, J.A., Garnica, W.T., Smith, D.G., Houghton, P., Lerche, N., Kanthaswamy, S., 2013. Singlenucleotide polymorphisms reveal patterns of allele sharing across the species boundary between rhesus (*macaca mulatta*) and cynomolgus (*m. fascicularis*) macaques. *Am. J. Primatol.* 75, 135–144.
- Scott, J.A., Grayson, D., Fletcher, E., Lee, A., Bauman, M.D., Schumann, C.M., Buonocore, M.H., Amaral, D.G., 2016. Longitudinal analysis of the developing rhesus monkey brain using magnetic resonance imaging: birth to adulthood. *Brain Struct. Funct.* 221, 2847–2871.
- Seiditz, J., Sponheim, C., Glen, D., Frank, Q.Y., Saleem, K.S., Leopold, D.A., Ungerleider, L., Messinger, A., 2018. A population MRI brain template and analysis tools for the macaque. *Neuroimage* 170, 121–131.
- Shen, S., Szameitat, A.J., Sterr, A., 2007. VBM lesion detection depends on the normalization template: a study using simulated atrophy. *Magn. Reson. Imaging* 25, 1385–1396.
- Shi, Y., Budin, F., Yapuncich, E., Rumble, A., Young, J.T., Payne, C., Zhang, X., Hu, X., Godfrey, J., Howell, B., et al., 2017. Unc-emory infant atlases for macaque brain image analysis: postnatal brain development through 12 months. *Front. Neurosci.* 10, 617.
- Shi, F., Wang, L., Wu, G., Gilmore, J.H., Lin, W., Shen, D., 2014. Neonatal atlas construction using sparse representation. *Human Brain Mapping* doi:10.1002/hbm.22502.
- Song, X., Garcia-Saldivar, P., Kindred, N., Wang, Y., Merchant, H., Meguerditchian, A., Yang, Y., Stein, E.A., Bradberry, C.W., Hamed, S.B., 2021. Strengths and challenges of longitudinal non-human primate neuroimaging. *Neuroimage* 118009.
- Sóskuthy, M., 2017. Generalised additive mixed models for dynamic analysis in linguistics: a practical introduction. *arXiv preprint arXiv:1703.05339*.
- Styner, M., Knickmeyer, R., Joshi, S., Coe, C., Short, S.J., Gilmore, J., 2007. Automatic Brain Segmentation in Rhesus Monkeys. In: *Proceedings of the Medical Imaging 2007: Image Processing*. International Society for Optics and Photonics, p. 65122L.
- Sun, Y., Gao, K., Wu, Z., Li, G., Zong, X., Lei, Z., Wei, Y., Ma, J., Yang, X., Feng, X., et al., 2021. Multi-site infant brain segmentation algorithms: the ISEG-2019 challenge. *IEEE Trans. Med. Imaging* 40, 1363–1376.
- Sussman, D., Leung, R.C., Chakravarty, M.M., Lerch, J.P., Taylor, M.J., 2016. The developing human brain: age-related changes in cortical, subcortical, and cerebellar anatomy. *Brain Behav.* 6, e00457.
- Tustison, N.J., Avants, B.B., 2013. Explicit b-spline regularization in diffeomorphic image registration. *Front. Neuroinform.* 7, 39.
- Tustison, N.J., Avants, B.B., Cook, P.A., Zheng, Y., Egan, A., Yushkevich, P.A., Gee, J.C., 2010. N4itk: improved N3 bias correction. *IEEE Trans. Med. Imaging* 29, 1310–1320.
- Uematsu, A., Matsui, M., Tanaka, C., Takahashi, T., Noguchi, K., Suzuki, M., Nishijo, H., 2012. Developmental trajectories of amygdala and hippocampus from infancy to early adulthood in healthy individuals. *PLoS ONE* 7, e46970.
- Usus, A., Grigorescu, I., Pietsch, M., et al., 2021. Multi-channel 4D parametrized Atlas of Macro- and Microstructural Neonatal Brain Development. *Frontiers in Neuroscience* doi:10.3389/fnins.2021.661704.
- Van Essen, D.C., 2004. Surface-based approaches to spatial localization and registration in primate cerebral cortex. *Neuroimage* 23, S97–S107.
- Van Essen, D.C., Dierker, D.L., 2007. Surface-based and probabilistic atlases of primate cerebral cortex. *Neuron* 56, 209–225.
- Wang, F., Lian, C., Xia, J., Wu, Z., Duan, D., Wang, L., Shen, D., Li, G., 2018. Construction of spatiotemporal infant cortical surface atlas of Rhesus Macaque. In: *Proceedings of the IEEE 15th International Symposium on Biomedical Imaging (ISBI 2018)*. IEEE, pp. 704–707.
- Wang, F., Lian, C., Wu, Z., Zhang, H., Li, T., Meng, Y., Lin, W., Shen, D., Li, G., 2019. Developmental topography of cortical thickness during infancy. *Proceedings of the National Academy of Sciences of the United States of America* doi:10.1073/pnas.1821523116.
- Wang, J., Vachet, C., Rumble, A., Gouttard, S., Ouziel, C., Perrot, E., Du, G., Huang, X., Gerig, G., Styner, M.A., 2014. Multi-atlas segmentation of subcortical brain structures via the autoseg software pipeline. *Front. Neuroinform.* 8, 7.
- Wang, L., Gao, Y., Shi, F., Li, G., Gilmore, J.H., Lin, W., Shen, D., 2015. Links: learning-based multi-source integration framework for segmentation of infant brain images. *Neuroimage* 108, 160–172.
- Weiss, A.R., Liu, Z., Wang, X., Liguori, W.A., Kroenke, C.D., McBride, J.L., 2020. The macaque brain ONPRC18 template with combined gray and white matter labelmap for multimodal neuroimaging studies of nonhuman primates. *Neuroimage* 225, 117517.
- Wu, Z., Wang, L., Lin, W., Gilmore, J.H., Li, G., Shen, D., 2019. Construction of 4d infant cortical surface atlases with sharp folding patterns via spherical patch-based group-wise sparse representation. *Hum. Brain Mapp.* 40, 3860–3880.
- Xia, J., Wang, F., Benkarim, O.M., Sanroma, G., Piella, G., Gonzlez Ballester, M.A., Hahn, N., Eixarch, E., Zhang, C., Shen, D., 2019. Fetal cortical surface atlas parcellation based on growth patterns. *Hum. Brain Mapp.* 40, 3881–3899.
- Xia, J., Wang, F., Wu, Z., Wang, L., Zhang, C., Lin, W., Shen, D., Li, G., 2019. Charting Development-Based Joint Parcellation Maps Of Human and Macaque Brains During Infancy. *16th IEEE International Symposium on Biomedical Imaging*. IEEE.
- Xia, J., Wang, F., Wu, Z., Wang, L., Zhang, C., Shen, D., Li, G., 2020. Mapping hemispheric asymmetries of the macaque cerebral cortex during early brain development. *Hum. Brain Mapp.* 41, 95–106.
- Yan, G., Zhang, G., Fang, X., Zhang, Y., Li, C., Ling, F., Cooper, D.N., Li, Q., Li, Y., Van Gool, A.J., 2011. Genome sequencing and comparison of two nonhuman primate animal models, the cynomolgus and Chinese rhesus macaques. *Nat. Biotechnol.* 29, 1019–1023.
- Yoon, U., Fonov, V.S., Perusse, D., Evans, A.C., Group, B.D.C., 2009. The effect of template choice on morphometric analysis of pediatric brain data. *Neuroimage* 45, 769–777.
- Yushkevich, P.A., Piven, J., Hazlett, H.C., Smith, R.G., Ho, S., Gee, J.C., Gerig, G., 2006. User-guided 3D active contour segmentation of anatomical structures: significantly improved efficiency and reliability. *Neuroimage* 31, 1116–1128.
- Zhong, T., Zhang, Y., Zhao, F., Pei, Y., Liao, L., Ning, Z., Wang, L., Shen, D., Li, G., 2021. Domain-invariant prior knowledge guided attention networks for robust skull stripping of developing macaque brains. In: *Proceedings of the International Conference on Medical Image Computing and Computer-Assisted Intervention*. Springer, pp. 22–32.
- Zhong, T., Zhao, F., Pei, Y., Ning, Z., Liao, L., Wu, Z., Niu, Y., Wang, L., Shen, D., Zhang, Y., 2021. Dika-nets: domain-invariant knowledge-guided attention networks for brain skull stripping of early developing macaques. *Neuroimage* 227, 117649.